

## RESEARCH LETTER

10.1002/2016GL071891

## Key Points:

- Phase separation near the magmatic heat source controls heat transfer efficiency in hydrothermal systems with saline fluids
- Phase separation above shallow intrusions is by boiling and produces hypersaline brines that reduce heat transfer
- Phase separation above deep intrusions is by condensation and maximizes heat transfer

## Supporting Information:

- Supporting Information S1
- Data Set S1

## Correspondence to:

S. Scott,  
samuelwarrenscott@gmail.com

## Citation:

Scott, S., T. Driesner, and P. Weis (2017), Boiling and condensation of saline geothermal fluids above magmatic intrusions, *Geophys. Res. Lett.*, 44, doi:10.1002/2016GL071891.

Received 10 NOV 2016

Accepted 11 JAN 2017

Accepted article online 12 JAN 2017

## Boiling and condensation of saline geothermal fluids above magmatic intrusions

Samuel Scott<sup>1</sup> , Thomas Driesner<sup>1</sup> , and Philipp Weis<sup>2</sup> 

<sup>1</sup>Department of Earth Sciences, Institute of Geochemistry and Petrology, ETH Zurich, Zurich, Switzerland, <sup>2</sup>GFZ German Research Centre for Geosciences, Potsdam, Germany

**Abstract** Numerical simulation of subaerial, magma-driven, saline hydrothermal systems reveals that fluid phase separation near the intrusion is a first-order control on the dynamics and efficiency of heat and mass transfer. Above shallow intrusions emplaced at <2.5 km depth, phase separation through boiling of saline liquid leads to accumulation of low-mobility hypersaline brines and halite precipitation, thereby reducing the efficiency of heat and mass transfer. Above deeper intrusions (>4 km), where fluid pressure is >30 MPa, phase separation occurs by condensation of hypersaline brine from a saline intermediate-density fluid. The fraction of brine remains small, and advective, vapor-dominated mass and heat fluxes are maximized. We thus hypothesize that, in contrast to pure water systems, for which shallow intrusions make better targets for supercritical resource exploitation, the optimal targets in saline systems are located above deeper intrusions.

### 1. Introduction

Subsurface magmatic intrusions emplaced in the upper crust provide heat that drives hydrothermal systems, which are sites of major, focused heat transfer. They are the most favorable environments for the development of high-enthalpy geothermal resources [Moeck, 2014], and major types of hydrothermal ore deposits may form given appropriate conditions for metal input, flow focusing, and efficient metal precipitation mechanisms [Heinrich and Candela, 2014]. In most systems, the convecting fluid is dominantly meteoric water with minor input of magmatic volatiles like CO<sub>2</sub> and H<sub>2</sub>S [Henley and Ellis, 1983].

Magma-driven geothermal systems often develop conditions of liquid-vapor coexistence (i.e., "boiling") in their upflow zones [Arnórsson *et al.*, 2007]. The vertical extent and thermal structure of boiling zones are primarily controlled by the permeability of the host rock, the depth of the intrusion, and the temperature dependence of permeability around the intrusion, which reflects the brittle-ductile transition in the host rock [Hayba and Ingebritsen, 1997; Scott *et al.*, 2016]. In systems with meteoric-derived, dilute water, liquid-vapor phase separation is limited to pressures and temperatures below the critical point of water (22.055 MPa/373.976°C) [Haar *et al.*, 1984]. At higher temperatures and pressures, such systems may develop economically interesting, supercritical geothermal resources above the magma [Scott *et al.*, 2015], which were encountered in the Iceland Deep Drilling Project (IDDP) well 1 at the Krafla volcano [Elders *et al.*, 2014].

Several active high-enthalpy geothermal systems, such as Reykjanes in Iceland [Arnórsson, 1978] or Salton Sea in California [Helgeson, 1968], feature geothermal waters containing significant concentrations of dissolved salt. Saline water phase relations, approximated by the system H<sub>2</sub>O-NaCl, differ significantly from those of pure water, and liquid-vapor coexistence can extend to temperatures and pressures far above the critical values of pure water [Sourirajan and Kennedy, 1962; Bischoff and Pitzer, 1989]. According to the topology of the H<sub>2</sub>O-NaCl phase diagram (Figure 1), heating may gradually transform a cool saline liquid into a hot, vapor-like fluid or result in a hot, liquid-like phase, depending on pressure [Heinrich *et al.*, 2004; Foustoukos and Seyfried, 2007]. Accordingly, when a heated fluid intersects the phase boundary of the region of liquid-vapor coexistence, phase separation will occur by condensation if pressure is higher than the critical pressure for the given salinity or by boiling if pressure is lower [Fournier, 1987; Geiger *et al.*, 2005]. Both styles have been shown to occur in the subsurface of mid-ocean ridge hydrothermal systems where pressures are sufficiently high [Bischoff and Rosenbauer, 1987; Foustoukos and Seyfried, 2007; Coumou *et al.*, 2009]. In subaerial saline hydrothermal systems, however, pressures are generally lower due to the lack of an overlying seawater column, and intense phase separation by condensation has so far not been described.

In the following, we present transient simulations of convection of H<sub>2</sub>O-NaCl fluids around magmatic intrusions, which demonstrate that both styles of phase separation can occur in the deep parts of saline

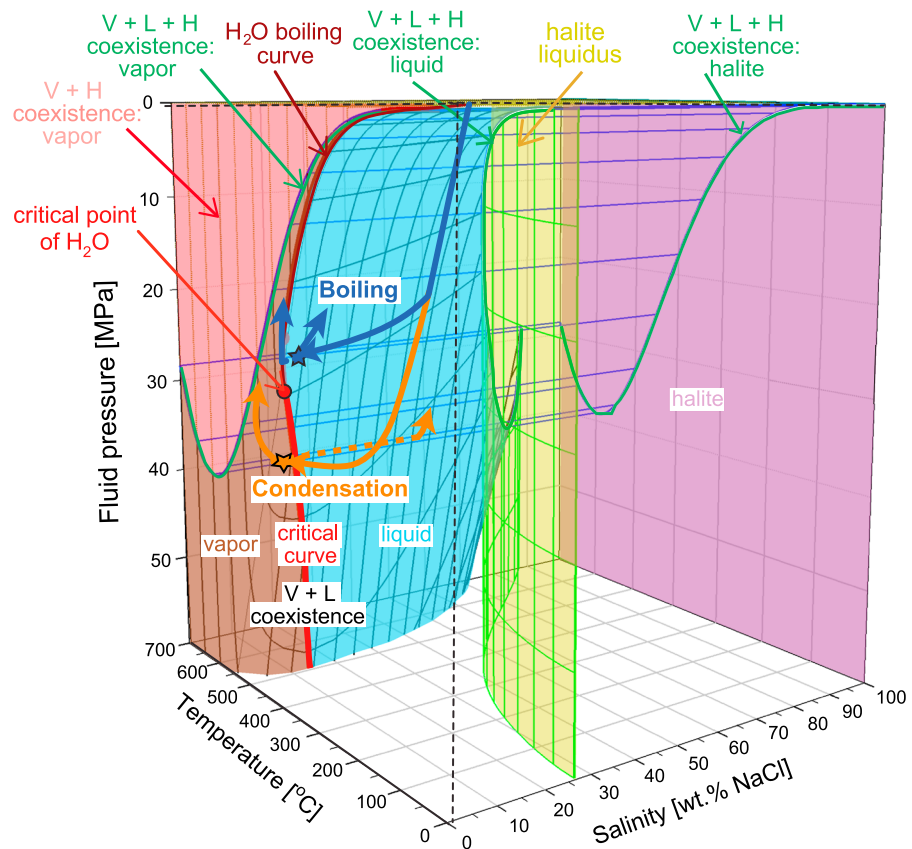


**Figure 1.** Phase diagram of the system  $\text{H}_2\text{O-NaCl}$  [Driesner and Heinrich, 2007] illustrating the effect of intrusion depth on the style of phase separation of an initial seawater-salinity fluid. The blue path represents the circulation from the surface to  $\sim 2.5$  km depth, followed by upflow and boiling, while the orange path represents the circulation to  $\sim 4.5$  km depth, followed by upflow and condensation.

geothermal systems near the intrusion. We analyze how the near-intrusion interplay of heat transfer, fluid flow, and saline fluid phase relations governs the physical hydrology, the efficiency of heat transport, and the development of different styles of geothermal resources. Heat transport is maximized within condensation zones, which only form in subaerial systems if the intrusion is sufficiently deep ( $>\sim 4$  km). In contrast, hypersaline brines accumulate within boiling zones above shallower intrusions and hamper heat transfer efficiency due to their high density and low mobility.

## 2. Methods

The governing equations of mass and energy conservation for multiphase flow of  $\text{H}_2\text{O-NaCl}$  fluids are solved using a continuum, porous medium approach with a pressure-enthalpy-based formulation in a Control Volume Finite Element Method numerical scheme using the Complex Systems Modeling Platform (CSMP++). The computational approach has been described in detail by *Weis et al.* [2014] and is thus only briefly summarized in Text S1 in the supporting information, along with boundary and initial conditions in Text S2.

### 2.1. Model Setup

The simulations describe the development of a saline geothermal system within a two-dimensional vertical section above a magmatic body intruded into host rocks with a permeability of  $10^{-15} \text{ m}^2$  initially containing pore waters with seawater salinity. We choose this permeability value because previous studies have shown that it is common in natural systems [Björnsson and Bödvarsson, 1990; Manning and Ingebritsen, 1999] and close to optimal for the formation of spatially extensive supercritical geothermal resources in pure water systems [Scott et al., 2015, 2016]. We performed simulations testing possible conditions for the Reykjanes

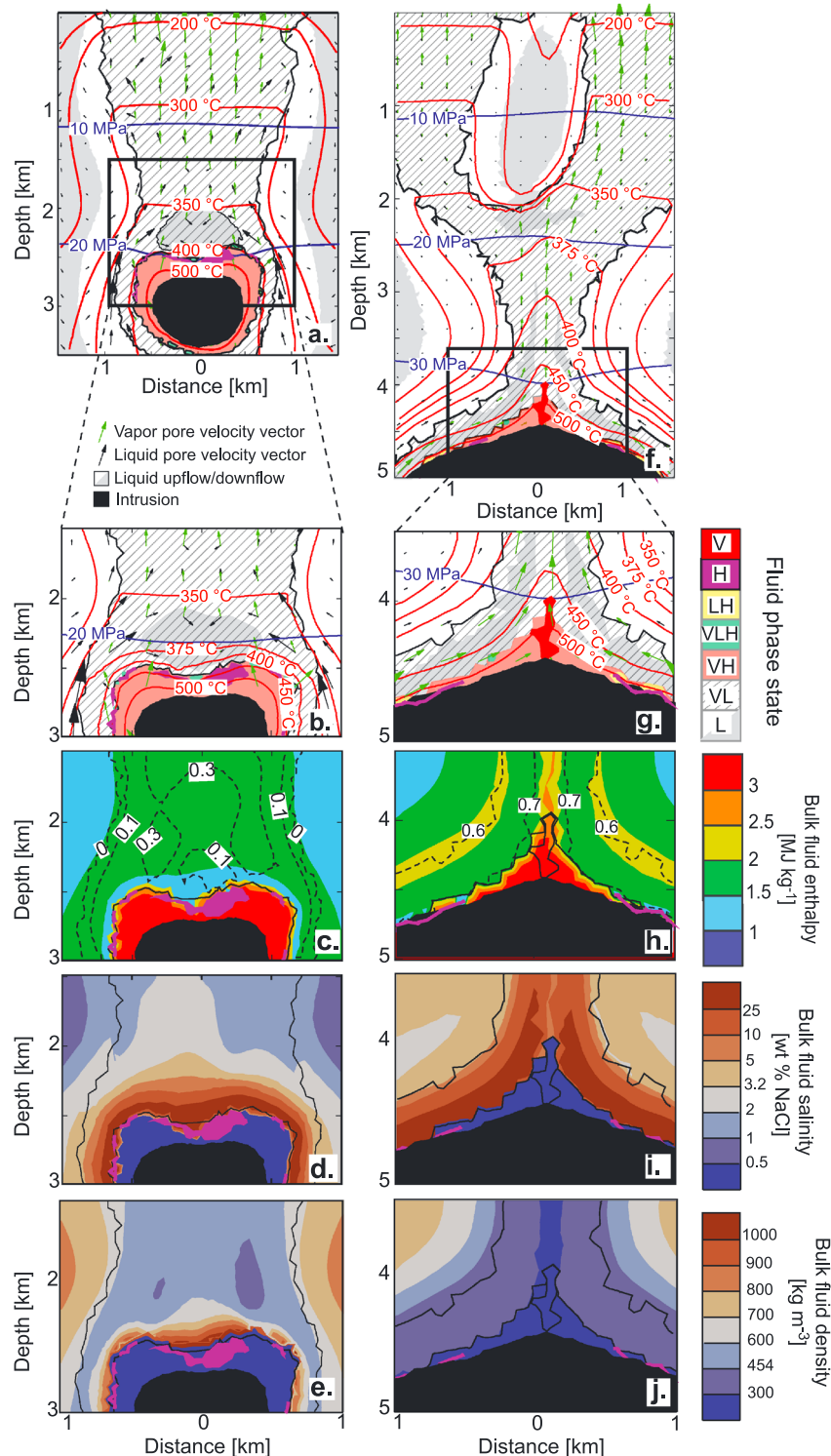


**Figure 2.** The thermal structure of saline geothermal systems. (a and f) Large-scale system structure for systems with shallow (2.5 km depth) or deep (4.5 km) intrusions after 3600 and 7000 years of system evolution, respectively, are shown, with fluid phase state (see text), isotherms (red lines), isobars (blue lines), and liquid and vapor pore velocity vectors (black and green, respectively). Areas where the vertical component of the liquid flow is oriented upward or downward are colored in white or grey, respectively. The location of the intrusion, defined by having a permeability of  $<10^{-16} \text{ m}^2$ , is shown in black. Snapshots show the (b and g) fluid phase state, (c and h) vapor volumetric saturation (dashed lines) and bulk fluid enthalpy, (d and i) bulk fluid salinity, and (e and j) bulk fluid density. The area of the snapshots showing the excerpts in Figures 2b–2e and 2g–2j are shown by the black boxes in Figures 2a and 2f, respectively.

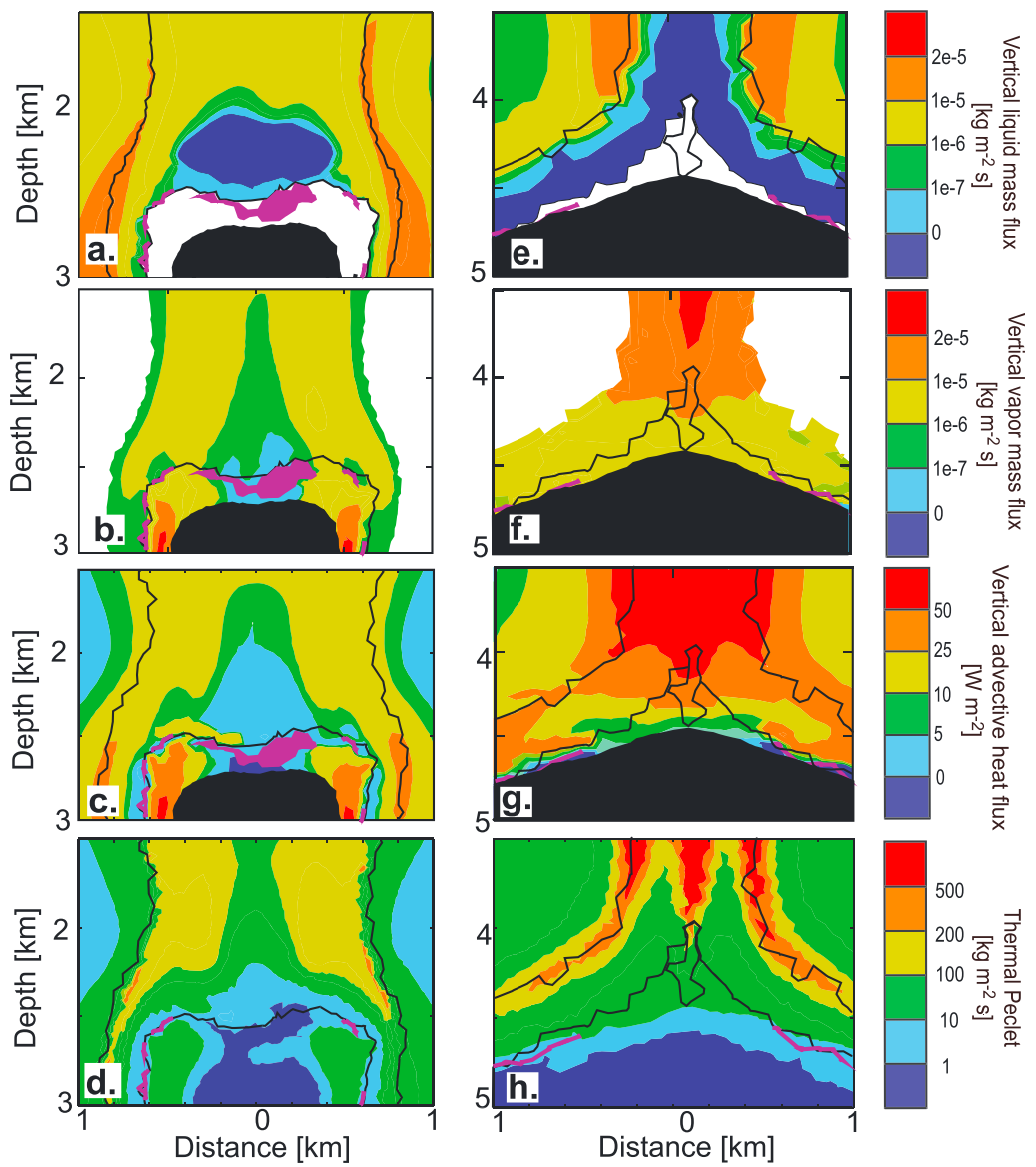


**Figure 3.** Vertical liquid and vapor and advective heat fluxes by thermohaline convection above intrusions. Snapshots show the (a and e) distribution of vertical liquid mass fluxes, (b and f) vertical vapor mass fluxes, (c and g) vertical advective heat flux, and (d and h) thermal Peclet number for systems with (Figures 3a–3d) shallow or (Figures 3e–3h) deep intrusion emplacement depth and  $T_{\text{BDT}}$  of 550°C. The intrusion is shown in black, and halite zones are shown in purple.

system, in which intrusion depth and brittle-ductile transition temperature are treated as variables. As this system is subaerial, we assume that recharge through the surface during the simulation is dominated by meteoric water of zero salinity. This is a simplification for the Reykjanes geothermal system, which is dominantly recharged by seawater entering from the nearby shores of the Reykjanes Peninsula [Arnórsson, 1978]. However, test simulations of initial seawater salinity systems with seawater influx at the top boundary suggest that the salinity of recharging waters only has a minor effect on the dynamics of hypersaline brine development and the salinity redistribution near the intrusion. Isotopic signatures do not indicate any contribution from magmatic fluids to the hydrothermal systems at Reykjanes [Pope *et al.*, 2009].

We use a temperature-dependent permeability [Hayba and Ingebritsen, 1997] to mimic permeability reduction due to the brittle-ductile transition (BDT) of rock around the intrusion [Fournier, 1999]. Permeability decreases above the onset temperature of the BDT,  $T_{\text{BDT}}$ , which was chosen here as 550°C based on experimental evidence of brittle deformation around this temperature range in basaltic rocks [Violay

*et al.*, 2012, 2015]. The effect of latent heat of crystallization is taken into consideration with a temperature-dependent rock heat capacity, which doubles from  $880 \text{ J kg}^{-1} \text{ }^{\circ}\text{C}^{-1}$  at temperatures below  $650^{\circ}\text{C}$  to  $1760 \text{ J kg}^{-1} \text{ }^{\circ}\text{C}^{-1}$  at temperatures greater than  $700^{\circ}\text{C}$ . Other initial rock properties are presented in Table S1. We vary intrusion emplacement depth (defined as the depth to the top of the intrusion) from 2.5 km to 4.5 km. The shallow intrusion initially has an elliptical geometry with horizontal and vertical axis lengths of 2 and 1 km, respectively, centered in a model domain 15 km wide and with 5 km vertical depth (Figure S1 in the supporting information). For the simulations with a deeper intrusion, we double the length of the axes to ensure that the system reaches a configuration where boiling occurs at the surface before the intrusion cools completely, in a model domain of 19 km width and 8 km vertical depth. Intrusion geometry only has a minor effect on the thermal structure of pure water systems [Scott *et al.*, 2016]. We simulate a single, instantaneous intrusion with subsequent transient cooling in response to heat conduction and convective heat transport by the circulating fluids. Repeated intrusions and magma chamber replenishment are ignored.

Saline fluids may reach saturation with a solid halite phase, which is assumed to reduce the available permeability for the mobile phases. A linear relative permeability model is applied with a vapor residual saturation of zero and liquid residual saturation of  $0.3(1 - S_h)$ , where  $S_h$  is the volumetric saturation of halite [Weis *et al.*, 2014]. Once the liquid saturation is below residual, two-phase flow theory considers liquid to be immobile [e.g., Ingebritsen *et al.*, 2006]. Halite is assumed to be immobile once precipitated, although it can be redissolved by later circulating fluids.

## 2.2. Phase Relations in the System $\text{H}_2\text{O-NaCl}$

All fluid properties needed for computation and analyses are calculated according to Driesner and Heinrich [2007] and Driesner [2007]. Under geothermal conditions, the system  $\text{H}_2\text{O-NaCl}$  (Figure 1) exhibits seven different combinations of the possible phase states vapor (V), liquid (L), and halite (H):

1. VL: The VL surface describes the compositions of coexisting liquid and vapor at a given pressure and temperature. At temperatures below the critical temperature of pure water, the crest of the VL surface is the pure  $\text{H}_2\text{O}$  boiling curve. At higher temperatures, the crest of the VL surface is the critical curve, which defines a locus of pressure-temperature-salinity ( $P$ - $T$ - $X$ ) conditions at which liquid and vapor have identical properties. For a given temperature, the critical curve specifies the maximum pressure of vapor-liquid coexistence.
2. L: In the present context, L is a fluid with liquid-like properties in terms of density and enthalpy. In the single-phase domain at pressures above the VL surface, fluid properties can continuously vary between vapor- and liquid-like without any heterogeneous phase change. Therefore, the distinction between liquid and vapor is based on convention, most commonly by defining fluids with a density less than that on the critical curve for the given salinity as vapor and those with a higher density as liquid [Liebscher and Heinrich, 2007]. Liquid-like properties are generally encountered at high salinities, low temperatures, and high pressures within the single-phase domain.
3. V: Following the same convention, fluid in the single-phase domain exhibits vapor-like properties at low salinities, high temperatures, and low pressures. Visualizations in Figures 2 and 3 use a slightly different, computationally pragmatic convention that defines “vapor” as a fluid with a salinity and pressure less than the critical values for a given temperature.
4. VLH: The vapor + liquid + halite surface forms the low-pressure boundary of VL coexistence. The maximum pressure of VLH coexistence is  $\sim 39 \text{ MPa}$  at  $\sim 595^{\circ}\text{C}$ .
5. VH: At pressures below the VLH surface, vapor coexists with solid halite.
6. LH: The composition of halite-saturated liquid as a function of pressure and temperature is given by the halite liquidus. The low-pressure boundary of the halite liquidus is the VLH surface.
7. H: In our simulations, we observe precipitation of halite in sufficient quantities for it to nearly or even completely saturate the pore space. In the visualizations, we label the phase state H when the volumetric saturation of halite in the pore space exceeds 0.95 to highlight nearly complete clogging of pore space.

The term “supercritical” can only be defined by convention and strictly so only for one-component fluids [Liebscher and Heinrich, 2007]; for dilute aqueous fluids, we proposed to define supercritical in relation to the temperature and enthalpy of the critical point of  $\text{H}_2\text{O}$ , irrespective of fluid pressure [Scott *et al.*, 2015].

In saline systems, such high-enthalpy, single-phase fluids are mostly restricted to the low-salinity, high-temperature part of the phase diagram.

### 3. Results

#### 3.1. Thermal Structure of Saline Geothermal Systems

The large-scale structure of a system driven by a shallow intrusion is shown in Figure 2a. Recharging liquid descends on the margins of the system (grey areas) toward the intrusion (black); the heated fluid ascends nearly vertically within an upflow plume (white areas), which show two-phase liquid-vapor (VL) zones extending to the depth of the intrusion. Fluid pressure above the intrusion is  $\sim 20$  MPa (Figure 2a). Halite-saturated vapor (VH) forms around the intrusion at temperatures  $\geq 400^\circ\text{C}$  (Figure 2b) and is enveloped on the outside by a VL zone. Halite volumetric saturations exceed 0.95 above the center of the intrusion (H; purple area). Near the central base of the plume and overlying the VH zone, a heat pipe configuration with downflowing liquid and upflowing vapor develops (Figure 2b). While the salinity and density of liquid along the outer edge of the VL zone is  $\sim 3$  wt % and  $\sim 600$  kg m $^{-3}$ , an increase to  $> 25$  wt % and 1000 kg m $^{-3}$  at the base of VL zone above the H zone (Figure 2e), along with a low bulk fluid enthalpy of  $< 1.5$  MJ kg $^{-1}$  (Figure 2c), indicates the accumulation of hypersaline brines at the base of the heat pipe zone.

A system with a deeper intrusion, emplaced at 4.5 km depth, shows vapor-rich upflow zones and, at fluid pressures  $> 30$  MPa near the intrusion, develops significant zones of phase separation by condensation (Figure 2f). In the deep parts, vapor saturation is  $> 0.6$  at the edge of the VL plume, and bulk fluid enthalpy is  $> 2$  MJ kg $^{-1}$  (Figure 2h). Halite-saturated vapor develops at  $> 500^\circ\text{C}$  and pressures below the maximum pressure of VH coexistence ( $\sim 39$  MPa) and is overlain by halite-undersaturated, single-phase vapor (V) at the center of the upflow plume (Figure 2f). Halite zones are narrow and restricted to the margins of the VH zone (Figure 2g). The enthalpy of single-phase vapor above the center of the intrusion is  $> 3$  MJ kg $^{-1}$ , and vapor saturation within the overlying VL zone is  $> 0.7$  (Figure 2h), thus implying that liquid is immobile. While bulk fluid salinity increases within the VL zone to  $> 25$  wt % at the boundary with the underlying VH zone, bulk fluid density is less than critical density of seawater ( $< 454$  kg m $^{-3}$ ) within the entire VL zone below 4 km depth (Figure 2j), an indication that the dominant mode of phase separation at these depths is condensation (Figure 1, orange lines) and that hypersaline brine does not accumulate in large amounts.

#### 3.2. Heat and Mass Transfer in Saline Geothermal Systems

The low mobility of dense, hypersaline brines at the base of the boiling plume reduces the effectiveness of convective heat loss from the top of shallow intrusions. The brine accumulation results from the downward liquid mass flux within the two-phase heat pipe at the base of the upflow plume (Figure 3a). At the interface with the underlying VH zone, liquid boils off to form solid halite and halite-saturated vapor. Importantly, upward vertical liquid mass fluxes are maximized along the cooler edges of the VL plume, where groundwater with a salinity close to that of seawater can actively circulate. Similarly, upward vertical vapor mass fluxes are higher near the edges of the VL plume and relatively low within the two-phase heat pipe at the base of the VL zone (Figure 3b). While bulk fluid enthalpy and rates of advective heat transfer may exceed 3 MJ kg $^{-1}$  and 50 W m $^{-2}$  within the VH zone, such conditions occur only along the sides of the intrusion where halite saturations are low. Vapor mass fluxes and heat transfer are strongly reduced within the halite-rich part of the VH zone above the center of the intrusion (Figure 3c). The efficiency of heat transfer can be expressed using the thermal Peclet number ( $Pe_T$ ), which measures the ratio of advective heat transfer to conductive heat transfer and is given by

$$Pe_T = \frac{\vec{v}_i S_i \rho_i h_i + \vec{v}_v S_v \rho_v h_v}{K \nabla T}$$

where  $\vec{v}_i$  denotes the Darcy velocity of fluid phase  $i$  (liquid l or vapor v),  $S$ ,  $h$ , and  $\rho$  refer to the volumetric saturation, specific enthalpy, and density of phase  $i$ ;  $K$  is the thermal conductivity of the rock, and  $T$  is the temperature. Maximum  $Pe_T$  of  $\sim 200$  are found along on the sides of the VL zone and decrease to  $< 10$  within the two-phase heat pipe above the center of the intrusion (Figure 3d). Heat transfer is conduction-dominated ( $Pe_T < 1$ ) within the H zone and the intrusion.

In contrast, vapor mass fluxes and rates of convective heat transfer are maximized within condensation zones above deep intrusions. Although these zones have lower liquid mass fluxes (Figure 3e), vapor mass fluxes are

comparatively high and maximized within the center of the upflow plume, where vapor from the underlying VH zone ascends (Figure 3f). As a result of the high vapor mass fluxes, vertical convective heat fluxes throughout this area are  $>50 \text{ W m}^{-2}$  (Figure 3g), in contrast to the generally lower values in shallower systems (Figure 3c). Much more efficient advective heat transfer within the condensation zone is indicated by the presence of a large area with  $Pe_7$  exceeding 500 (Figure 3h).

## 4. Discussion

### 4.1. Effect of Intrusion Depth on Style of Phase Separation

Magma emplacement depth determines the hot-hydrostatic fluid pressure above an intrusion and thereby controls whether saline fluid circulating above an intrusion undergoes phase separation by boiling or condensation. Increasing intrusion emplacement depth from  $\sim 2.5$  to  $4.5$  km shifts the hot-hydrostatic fluid pressure above an intrusion from values close to the critical pressure of pure water ( $P_{c,\text{H}_2\text{O}}$ ,  $\sim 22 \text{ MPa}$ ; Figure 2a) to  $>30 \text{ MPa}$ , close to the critical pressure of seawater (Figure 2f). While the boiling curve of pure water controls the maximum temperature of VL coexistence at pressures below  $P_{c,\text{H}_2\text{O}}$ , at higher pressures the maximum temperature of VL coexistence increases with increasing pressure along the  $\text{H}_2\text{O}-\text{NaCl}$  critical curve (Figure 1). Therefore, heated seawater circulating near shallow intrusions will remain liquid-like and phase separate by boiling at pressures less than the critical pressure of seawater. At depths of  $>4$  km, equivalent to hot-hydrostatic fluid pressures  $>30 \text{ MPa}$ , seawater can be heated to  $>400^\circ\text{C}$  without undergoing phase separation, attain an intermediate, vapor-like density lower than the critical density of seawater ( $\sim 450 \text{ kg m}^{-3}$ ; Figure 2j), and eventually phase separate by condensing small amounts of saline brine. Thus, fluids with seawater-like salinity will phase separate by boiling at low pressures above shallow intrusions and by condensation at high pressures above deep intrusions.

### 4.2. Effect of Phase Separation Style on Heat Transport

In the case of boiling, small fractions of low-salinity vapor nucleate out of a liquid-like fluid upon phase separation (Figure 1, blue lines). The low density of vapor causes it to ascend more rapidly than liquid in the buoyancy-driven convective field. Thus, vapor saturations are maintained at relatively low values in boiling zones above shallow intrusions. Two-phase heat pipes above the center of the intrusion are starved of less saline liquid, and low-enthalpy hypersaline brines accumulate, descend, and precipitate halite as liquid is progressively boiled off. Although vapor enthalpy exceeds  $>3 \text{ MJ kg}^{-1}$  around shallow intrusions, the near sealing of pore space resulting from the boiling off of hypersaline brines greatly reduces the accessible enthalpy contained in the pore space, as well as rates of advective heat transport.

During condensation, a small fraction of low-enthalpy hypersaline brine condenses out of a high-enthalpy, vapor-like fluid (Figure 1, orange lines). Higher vapor saturations decrease the relative permeability of liquid and increase the relative permeability of vapor, thereby allowing higher vapor mass fluxes. Condensation may occur in two different settings: (1) along the outer edges of deep VL zones, where intermediate-density fluid with a salinity close to that of seawater is heated, and (2) the center of the upflow plume below the base of the VL zone, where low-salinity vapor ascending from underlying VH zones depressurizes. The latter settings have vapor saturations  $>0.7$ , which indicate that the liquid brine is an immobile wetting phase. Thus, advective heat transfer within condensation zones is dominated by vapor advection, and to a lesser extent, heat conduction through the rock, which boils off liquid and maintains near-residual liquid saturations (Figure 3h). Vertical vapor mass fluxes and advective heat transport are highest within VL condensation zones at temperatures near  $400^\circ\text{C}$ , at which temperature the density of vapor is high [Klyukin *et al.*, 2016].

Although thermohaline convection increases the rate of heat loss from the intrusions relative to pure conduction, its effect on the cooling behavior of the intrusion depends strongly upon whether phase separation above the intrusion occurs by boiling or condensation. Boiling zones above shallow intrusions lead to accumulation of dense hypersaline brine and halite precipitation, both of which restrict fluid advection and thereby insulate the intrusion. Advective heat transport is much more efficient within condensation zones, where the rate of heat transfer can be increased relative to heat conduction-only by a factor of  $>200-500$  (Figure 3h). Thus, the process of phase separation by condensation enables saline geothermal systems to transport heat at an efficiency close to the maximum possible in pure water systems [Ingebretsen and Hayba, 1994; Coumou *et al.*, 2008]. Moreover, contrasting styles of phase separation may explain variations

in observed black-smoker salinities [Coulomou *et al.*, 2009], since systems with deep condensation zones have more vapor-rich and lower-salinity upflow zones compared to shallow intrusions with high-salinity brines (Figures 2d and 2i).

#### 4.3. Sealing of Pore Space by Halite Precipitation

Halite precipitation from saline magmatic fluids has been observed in numerical models of magmatic hydrothermal systems [Weis *et al.*, 2012; Gruen *et al.*, 2014; Weis, 2015], inferred from fluid inclusion analyses [Lecumberri-Sánchez *et al.*, 2015], and has been observed in a deep geothermal well, including a concomitant permeability reduction [Hesshaus *et al.*, 2013]. Our simulations indicate that the extent of halite precipitation in saline geothermal systems depends on the intrusion emplacement depth and the style of phase separation. At the base of boiling zones around shallow intrusions, extensive halite precipitation from descending hypersaline brines may seal pore space in underlying VH zones, greatly reducing vapor mass fluxes and advective heat loss. Near deeper intrusions, narrow zones of halite precipitation occur on the margins of VH zones.

Hypersaline brines can reach VLH conditions by pressure decrease or temperature increase. Although fluid pressure increases slightly as the brines descend, temperature increases rapidly with increasing proximity to the intrusion and leads to boiling off of liquid and halite precipitation. Halite precipitation via this mechanism is not observed above deep intrusions, which have relatively low liquid saturations within deep VL zones. Further, increasing fluid pressure associated with deeper intrusion emplacement depth increases the salinity and temperature of VL coexistence (Figure 1, compare to Figures 2b and 2d). However, sufficient halite precipitation to close pore space can still occur in narrow zones on the edge of the intrusion, where deep circulating fluids ascend and depressurize to pressures less than the maximum pressure of VH coexistence (Figure 2f).

Our simulations show that halite precipitation may restrict flow of vapor in the upper part of a VH zone around a shallow intrusion. As a result of the near-complete closure of pore space by halite precipitation, heat transfer will be conduction dominated even within parts of the hydrothermal system where permeability is  $>10^{-16} \text{ m}^2$  and advection should dominate [Ingebretsen *et al.*, 2006]. However, our models do not consider that halite is more conductive than basalt [Clauser and Huenges, 1995], which could potentially increase conductive heat loss in areas where pore space is occupied by halite.

#### 4.4. Supercritical Geothermal Resource Formation

Saline geothermal resources with enthalpies and fluid properties comparable to those found at Krafla can only form if particular pressure-temperature-salinity conditions are matched. The IDDP is currently drilling a second well to explore whether such conditions occur in the deep parts of the Reykjanes system [Friðleifsson *et al.*, 2014]. Our simulations show that high-enthalpy vapor resources form in saline geothermal systems around shallow intrusions at  $>400^\circ\text{C}$  and around deep intrusions at  $>500^\circ\text{C}$ . In geothermal systems containing pure water, supercritical resources at shallow depths are inferred to be optimal for exploitation, since the enthalpy of supercritical vapor at a given temperature increases with decreasing pressure [Scott *et al.*, 2015]. However, extensive halite precipitation and overlying hypersaline brines may reduce the attractiveness of VH zones around shallow intrusions in saline geothermal systems. Although heat transfer is most efficient within the condensation zone, an underlying VH or V zone with enthalpies  $>3 \text{ MJ kg}^{-1}$  may provide attractive geothermal resources.

### 5. Conclusions

Numerical simulations of subsurface flow of seawater-derived pore fluids around magmatic intrusions reveal several controls on the thermal structure of saline high-enthalpy geothermal systems:

1. Intrusion emplacement depth controls whether phase separation in the vicinity of an intrusion is dominantly carried out by boiling, as is the case for shallow intrusions, or by condensation, as occurs locally above deep intrusions at 4–5 km depth.
2. Whereas the accumulation of hypersaline brines in boiling zones above shallow intrusions reduces advective heat transport, the efficiency of heat transport is optimized within condensation zones near deep intrusions.
3. Halite precipitation from downward descending hypersaline brines may seal pore space.

**Acknowledgments**

We thank S. Ingebritsen and an anonymous reviewer for their insightful comments that helped to improve the manuscript. We further thank the development community of the CSMP++ platform, which has been used for this study and is subject to licensing through ETH Zurich, Heriot Watt University, and Montanuniversität Leoben. Unprocessed model output data are available online as zipped archives (Data Sets S1 and S2 in the supporting information). This study was funded by the Swiss National Science Foundation (CRSII2\_141843/1, Sinergia COTHERM). The authors declare no competing financial interests.

**References**

Arnórsson, S. (1978), Major element chemistry of the geothermal sea-water at Reykjanes and Svartsengi, Iceland, *Mineral. Mag.*, 42(322), 209–220, doi:10.1180/minmag.1978.042.322.07.

Arnórsson, S., A. Stefansson, and J. Ó. Bjarnason (2007), Fluid-fluid interactions in geothermal systems, *Rev. Mineral. Geochem.*, 65(1), 259–312, doi:10.2138/rmg.2007.65.9.

Bischoff, J., and K. Pitzer (1989), Liquid-vapor relations for the system NaCl-H<sub>2</sub>O: Summary of the P-T-x surface from 300 to 500°C, *Am. J. Sci.*, 289, 217–248.

Bischoff, J., and R. J. Rosenbauer (1987), Phase separation in seafloor hydrothermal systems: An experimental study on the effects on metal transport, *Am. J. Sci.*, 287, 953–978.

Björnsson, G., and G. Bödvarsson (1990), A survey of geothermal reservoir properties, *Geothermics*, 19(1), 17–27.

Clauzer, C., and E. Huenges (1995), Thermal conductivity of rocks and minerals, in *Rock Physics and Phase Relations: A Handbook of Physical Constants*, vol. 3, pp. 105–125, AGU, Washington, D. C.

Coumou, D., T. Driesner, and C. A. Heinrich (2008), Heat transport at boiling, near-critical conditions, *Geofluids*, 8(3), 208–215, doi:10.1111/j.1468-8123.2008.00218.x.

Coumou, D., T. Driesner, P. Weis, and C. A. Heinrich (2009), Phase separation, brine formation, and salinity variation at Black Smoker hydrothermal systems, *J. Geophys. Res.*, 114, B03212, doi:10.1029/2008JB005764.

Driesner, T. (2007), The system H<sub>2</sub>O-NaCl. Part II: Correlations for molar volume, enthalpy, and isobaric heat capacity from 0 to 1000°C, 1 to 5000 bar, and 0 to 1 X<sub>NaCl</sub>, *Geochim. Cosmochim. Acta*, 71(20), 4902–4919, doi:10.1016/j.gca.2007.05.026.

Driesner, T., and C. A. Heinrich (2007), The system H<sub>2</sub>O-NaCl. Part I: Correlation formulae for phase relations in temperature–pressure–composition space from 0 to 1000°C, 0 to 5000 bar, and 0 to 1 X<sub>NaCl</sub>, *Geochim. Cosmochim. Acta*, 71(20), 4880–4901, doi:10.1016/j.gca.2006.01.033.

Elders, W. A., G. Ó. Friðleifsson, and A. Albertsson (2014), Drilling into magma and the implications of the Iceland Deep Drilling Project (IDDP) for high-temperature geothermal systems worldwide, *Geothermics*, 49, 111–118, doi:10.1016/j.geothermics.2013.05.001.

Fournier, R. (1999), Hydrothermal processes related to movement of fluid from plastic into brittle rock in the magmatic-epithermal environment, *Econ. Geol.*, 94(8), 1193–1212.

Fournier, R. O. (1987), Conceptual models of brine evolution in magmatic-hydrothermal systems, in *Volcanism in Hawaii, US Geol. Surv. Prof. Pap.*, 1350, pp. 1487–1506.

Foustoukos, D. I., and W. E. Seyfried (2007), Fluid phase separation processes in submarine hydrothermal systems, *Rev. Mineral. Geochem.*, 65(1), 213–239, doi:10.2138/rmg.2007.65.7.

Friðleifsson, G. Ó., Ó. Sigríðsson, D. Thorbjörnsson, R. Karlssdóttir, Þ. Gíslason, A. Albertsson, and W. A. Elders (2014), Preparation for drilling well IDDP-2 at Reykjanes, *Geothermics*, 49, 119–126, doi:10.1016/j.geothermics.2013.05.006.

Geiger, S., T. Driesner, C. A. Heinrich, and S. K. Matthäi (2005), On the dynamics of NaCl-H<sub>2</sub>O fluid convection in the Earth's crust, *J. Geophys. Res.*, 110, B07101, doi:10.1029/2004JB003362.

Gruen, G. P., P. Weis, T. Driesner, C. A. Heinrich, and C. E. J. de Ronde (2014), Hydrodynamic modeling of magmatic–hydrothermal activity at submarine arc volcanoes, with implications for ore formation, *Earth Planet. Sci. Lett.*, 404, 307–318, doi:10.1016/j.epsl.2014.07.041.

Haar, L., J. S. Gallagher, and G. Kell (1984), *NBS/NRC Steam Tables*, Hemisphere, New York.

Hayba, D. O., and S. E. Ingebritsen (1997), Multiphase groundwater flow near cooling plutons, *J. Geophys. Res.*, 102(B6), 12,235–12,252, doi:10.1029/97JB00552.

Heinrich, C. A., and P. A. Candela (2014), Fluids and ore formation in the Earth's crust, in *Treatise on Geochemistry*, 2nd ed., edited by H. D. Holland and K. K. Turekian, pp. 1–28, Elsevier, Oxford.

Heinrich, C. A., T. Driesner, A. Stefánsson, and T. M. Seward (2004), Magmatic vapor contraction and the transport of gold from the porphyry environment to epithermal ore deposits, *Geology*, 32(9), 761, doi:10.1130/G20629.1.

Helgeson, H. C. (1968), Geologic and thermodynamic characteristics of the Salton Sea geothermal system, *Am. J. Sci.*, 266, 129–166.

Henley, R. W., and A. J. Ellis (1983), Geothermal systems ancient and modern: A geochemical review, *Earth Sci. Rev.*, 19(1), 1–50, doi:10.1016/0012-8252(83)90075-2.

Hesshaus, A., G. Houben, and R. Kringel (2013), Halite clogging in a deep geothermal well—Geochemical and isotopic characterisation of salt origin, *Phys. Chem. Earth*, 64, 127–139, doi:10.1016/j.pce.2013.06.002.

Ingebritsen, S. E., and D. O. Hayba (1994), Fluid flow and heat transport near the critical point of H<sub>2</sub>O, *Geophys. Res. Lett.*, 21, 2199–2202, doi:10.1029/94GL02002.

Ingebritsen, S. E., W. Sanford, and C. E. Neuzil (2006), *Groundwater in Geologic Processes*, 2nd ed., Cambridge Univ. Press, New York.

Klyukin, Y., T. Driesner, M. Steele-MacInnis, R. P. Lowell, and R. J. Bodnar (2016), Effect of salinity on mass and energy transport by hydrothermal fluids based on the physical and thermodynamic properties of H<sub>2</sub>O-NaCl, *Geofluids*, doi:10.1111/gfl.12181.

Lecumberri-Sánchez, P., M. Steele-MacInnis, P. Weis, T. Driesner, and R. J. Bodnar (2015), Salt precipitation in magmatic-hydrothermal systems associated with upper crustal plutons, *Geology*, 43(12), G37163.1, doi:10.1130/G37163.1.

Liebscher, A., and C. A. Heinrich (2007), Fluid-fluid interactions in the Earth's lithosphere, *Rev. Mineral. Geochem.*, 65(1), 1–13, doi:10.2138/rmg.2007.65.1.

Manning, C. E., and S. E. Ingebritsen (1999), Permeability of the continental crust: Implications of geothermal data and metamorphic systems, *Rev. Geophys.*, 37(1), 127–150, doi:10.1029/1998RG900002.

Moek, I. S. (2014), Catalog of geothermal play types based on geologic controls, *Renew. Sustain. Energy Rev.*, 37, 867–882, doi:10.1016/j.rser.2014.05.032.

Pope, E. C., D. K. Bird, S. Arnórsson, T. Friðriksson, W. A. Elders, and G. Ó. Friðleifsson (2009), Isotopic constraints on ice age fluids in active geothermal systems: Reykjanes, Iceland, *Geochim. Cosmochim. Acta*, 73, 4468–4488, doi:10.1016/j.gca.2009.03.033.

Scott, S., T. Driesner, and P. Weis (2015), Geologic controls on supercritical geothermal resources above magmatic intrusions, *Nat. Commun.*, 6, 7837, doi:10.1038/ncomms8837.

Scott, S., T. Driesner, and P. Weis (2016), The thermal structure and temporal evolution of high-enthalpy geothermal systems, *Geothermics*, 62, 33–47, doi:10.1016/j.geothermics.2016.02.004.

Sourirajan, S., and G. C. Kennedy (1962), The system H<sub>2</sub>O-NaCl at elevated temperatures and pressures, *Am. J. Sci.*, 260, 115–141.

Violay, M., B. Gibert, D. Mainprice, B. Evans, J.-M. Dautria, P. Azais, and P. Pezard (2012), An experimental study of the brittle-ductile transition of basalt at oceanic crust pressure and temperature conditions, *J. Geophys. Res.*, 117, B03213, doi:10.1029/2011JB008884.

Violay, M., B. Gibert, D. Mainprice, and J.-P. Burg (2015), Brittle versus ductile deformation as the main control of the deep fluid circulation in oceanic crust, *Geophys. Res. Lett.*, 42, 2767–2773, doi:10.1002/2015GL063437.

Weis, P. (2015), The dynamic interplay between saline fluid flow and rock permeability in magmatic-hydrothermal systems, *Geofluids*, 15(1–2), 350–371, doi:10.1111/gfl.12100.

Weis, P., T. Driesner, and C. A. Heinrich (2012), Porphyry-copper ore shells form at stable pressure-temperature fronts within dynamic fluid plumes, *Science*, 338(6114), 1613–6, doi:10.1126/science.1225009.

Weis, P., T. Driesner, D. Coumou, and S. Geiger (2014), Hydrothermal, multiphase convection of H<sub>2</sub>O-NaCl fluids from ambient to magmatic temperatures: A new numerical scheme and benchmarks for code comparison, *Geofluids*, 14(3), 347–371, doi:10.1111/gfl.12080.